Orientation of alkyl chains and hindered rotation of carbonyl groups in the smectic-C^* phase of antiferroelectric liquid crystals studied by polarized Fourier transform infrared spectroscopy

Kyeong Hyeon Kim, Ken Ishikawa, Hideo Takezoe, and Atsuo Fukuda
Tokyo Institute of Technology, Department of Organic and Polymeric Materials, O-okayama, Meguro-ku, Tokyo 152, Japan
(Received 26 September 1994)

Several absorbance peaks in electrically unwound, uniform smectic-C^* (Sm-C^*) were studied as a function of polarization direction of incident ir radiation by using homogeneously and homeotropically aligned cells of four antiferroelectric liquid crystals. Contrary to the "zigzag model," the average stretching direction of phenyl rings and the average orientation of two alkyl chains are almost parallel to the long molecular axis. Carbonyl rotation in the chiral and core parts is confirmed to be hindered. The most probable orientation of each individual chiral carbonyl group is not in the plane containing the two-fold axis of the C_2 point group to which Sm-C^* belongs; the spontaneous polarization appears along the C_2 axis perpendicularly to the tilting plane because of head-and-tail equivalence. A possible orientational distribution, mirror symmetric with respect to the tilting plane, is suggested in connection with the hindered rotation of the core carbonyl group. The electric-field-induced phase transition between Sm-C_A^* and Sm-C^* was also investigated by an asynchronous time-resolved method; all the molecular segments reorient simultaneously in the microsecond time scale.

PACS number(s): 61.30.Gd, 77.80.−e, 78.30.−j

I. INTRODUCTION

Since the discovery of tristable switching between the antiferroelectric chiral smectic-C_A (Sm-C_A^*) phase and the ferroelectric chiral smectic-C (Sm-C^*) phase [1,2], a large number of investigations on Sm-C_A^*, Sm-C^*, and related subphases in several antiferroelectric liquid crystals have been performed to clarify their structure and the origin of their emergence. As a result of the investigations, the pair formation of transverse dipole moments in adjacent smectic layers and the packing entropy due to the excluded volume effect are considered important for the appearance of antiferroelectricity and ferroelectricity, respectively [3]. These two characteristics, the pair formation and the packing entropy, must be closely related to the molecular conformation and the rotation about the long molecular axis, particularly to the alkyl chain orientation with respect to the core and the hindered rotation of molecular segments located closely to the asymmetric carbon and responsible for transverse dipole moments [4–8].

For an investigation of the molecular conformation and hindered rotation, vibrational spectroscopy such as Fourier transform infrared (FTIR) and Raman scattering

For an investigation of the molecular conformation and hindered rotation, vibrational spectroscopy such as Fourier transform infrared (FTIR) and Raman scattering can be used as powerful tools. A particular advantage of using vibrational spectroscopy is the ability to obtain orientational information about selected groups if the transition moments are well defined; this can be determined by measuring the absorption of polarized incident radiation. Owing to the development of infrared (ir) spectrophotometric techniques [9–11], it becomes possible not only to obtain polarized ir spectra reliably but also to observe the reorientation dynamics of liquid crystals, which suggests an average alkyl chain orientation parallel to the long molecular axis and a hindered rotation of the carbonyl groups. The electric-field-induced reorientation dynamics were also investigated, though preliminarily, by an asynchronous time-resolved method [10].

II. EXPERIMENT

Four antiferroelectric liquid crystals were used in this experiment. The structural formulas of these materials and the phase sequences in the cooling processes are summarized in Table I. Homogeneously aligned samples were prepared between two indium tin oxide (ITO) (70 nm thick) coated SrF_2 plates (2 mm thick), which are transparent in the visible and ir regions (0.13–11 μm). These plates were spin coated by polyvinylalcohol or polyimide, and one of these was rubbed unidirectionally. Polyester films (2–5 μm thick) were used as spacers. Homeotropically aligned samples were also prepared by using the SrF_2 plates as substrates, and two sheets of aluminum foil (8 μm thick) as electrodes as well as spacers. The cell thickness was estimated from the interference pattern measured before introducing the sample. The prepared cells were placed in a temperature-controlling oven which had a maximum thermal fluctuation of ± 0.02 °C. The alignment quality was checked by a polarizing optical microscope.

Using a JEOL JIR-MICRO 6000 system equipped with a microattachment and an MCT detector, polarized ir spectra were measured as a function of polarizer rotation angle. A wire grid polarizer was used for obtaining polarized ir radiation, and it was rotated on the axis parallel to the propagation direction. The measurement geometries are schematically illustrated in Fig. 1. Since the chevron structure in antiferroelectric liquid crystals is

 ©1995 The American Physical Society

TABLE I. Structural formulas and phase sequences for several antiferroelectric liquid crystals used in this experiment.

(S) - MHPOBC $C_8H_{17}O$–⟨⟩–COO–⟨⟩–COO–$\dot{C}H(CH_3)C_6H_{13}$

Iso $\underset{148\,^\circ C}{\leftrightarrow}$ Sm-A $\underset{122\,^\circ C}{\leftrightarrow}$ Sm-C^*_α $\underset{120.9\,^\circ C}{\leftrightarrow}$ Sm-C^* $\underset{119.2\,^\circ C}{\leftrightarrow}$ Sm-C^*_γ $\underset{118.4\,^\circ C}{\leftrightarrow}$ Sm-C^*_A $\underset{65\,^\circ C}{\leftrightarrow}$ Cry

TFMNPOBC $C_8H_{17}O$–⟨⟩–COO–⟨⟩–COO–$\dot{C}H(CF_3)C_8H_{17}$

Iso $\underset{114\,^\circ C}{\leftrightarrow}$ Sm-A $\underset{103\,^\circ C}{\leftrightarrow}$ Sm-C^*_A

TFMHPDOPB $C_{12}H_{25}O$–⟨N,N⟩–COO–⟨⟩–COO–$\dot{C}H(CF_3)C_6H_{13}$

Iso $\underset{104\,^\circ C}{\leftrightarrow}$ Sm-A $\underset{97\,^\circ C}{\leftrightarrow}$ Sm-C^*_A $\underset{32\,^\circ C}{\leftrightarrow}$ Cry

TFMHPODB $C_8H_{17}O$–⟨O,O⟩–COO–⟨⟩–COO–$\dot{C}H(CF_3)C_6H_{13}$

Iso $\underset{80\,^\circ C}{\leftrightarrow}$ Sm-A $\underset{65\,^\circ C}{\leftrightarrow}$ Sm-C^*_A $\underset{10\,^\circ C}{\leftrightarrow}$ Cry

readily converted to a pseudobookshelf structure by applying an electric field [20], the layer and molecular orientational structures in homogeneously as well as homeotropically aligned cells are considered to be almost ideal, as illustrated in Figs. 1(a) and 1(b). A homeotropically aligned sample was also rotated on the axis parallel to the electric-field direction [the Y axis in Fig. 1(c)], when necessary for measurements using obliquely incident radiation. The measuring conditions were 4-cm^{-1} wave number resolution, 70-times repetition, and 6.4-mm/s scanning speed (moving mirror speed). In the case of the obliquely incident experiment, we also used a triglycine sulfate (TGS) detector with a slower scanning rate (1.03 mm/s) to attain a better signal to noise (S/N) ratio. The absorption bands arising from water vapor were subtracted in the spectra.

Time resolved measurements were also made using the FTIR system together with a boxcar integrator (Stanford Research, SR250 and SR280) consisting of a gate circuit, a pulse delay circuit, and a low pass filter. A 40-μs pulsed electric field of ± 48 V amplitude and 1-kHz repetition was applied on a homogeneously aligned cell by a function generator (Wavetek, Model 75) and an amplifier (NF, Model 4005). The gate of the boxcar integrator was opened for 1 μs after $1.5n$ ($n=0,1,2,\ldots$) microseconds from the voltage rise. Thus time-resolved ir spectra were measured from 0 to 85 μs at intervals of 1.5 μs. The speed of the moving mirror was set at 0.12 mm/s. The wave number resolution was 8 cm^{-1} and the intervals between the data points were 4 cm^{-1}. All measurements were accumulated 800 times. To compare the time-resolved FTIR spectra with the optical switching behavior, the transmittance of visible light was measured by using an optical microscope attached to the FTIR system.

III. EXPERIMENTAL RESULTS

A. Polarized ir spectra in Sm-A observed using homogeneously aligned cells

Figure 2(a) is a view of the polarized ir spectra as a function of polarizer rotation angle, ω, in Sm-A of a homogeneously aligned TFMHPODB (see Table I) cell. Here ω is the angle between the smectic layer normal and the polarization direction of an incident radiation, and is taken as zero when these two directions coincide with each other. To see more clearly the wave number dependence, the spectra at $\omega=0°$ and 90° are reproduced in Fig. 2(b). The assignments of several absorption peaks are listed in Table II. The peaks due to CH_3, CH_2, C=O, C—O, and phenyl ring stretching [21,22], CH_2 scissor, and aromatic CH deformation modes [21,23,24] are observed. The CF_3 stretching peak [21], which should appear in the frequency range between 1000 and 1400 cm^{-1}, is probably buried under other strong peaks. The C=O stretching peaks due to the two carbonyls in the chiral and core parts are not separated because of the inductive effect [21,22] of CF_3 in the chiral part. In the case of compounds like MHPOBC (see Table I), which have CH_3 instead of CF_3, the two C=O stretching peaks are well separated. The peak due to C=O in the core part is observed at 1739 cm^{-1}, and the one in the chiral part appears at 1720 cm^{-1} in MHPOBC [25].

To see more clearly the polarization dependence, the peak absorbance is plotted as a function of ω, as illustrated in Fig. 3. The polarization dependence of the absorbance peaks will be conveniently described by circular graphs in the following, as shown in Fig. 4. A distance from the center represents the absorbance at a polarizer

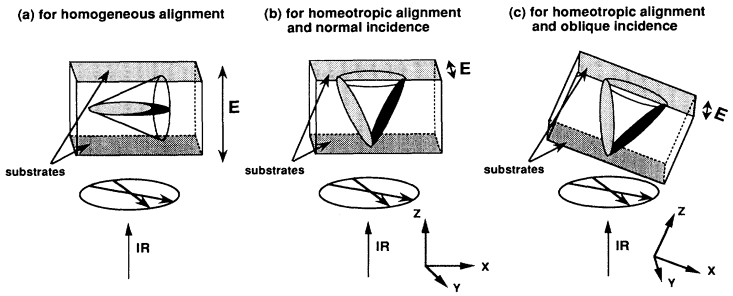

FIG. 1. Geometries used in polarized ir measurements for (a) homogeneously and (b) and (c) homeotropically aligned samples. For the oblique incidence of the radiation, the homeotropically aligned samples were rotated on the Y axis as illustrated in (c). Here the Y and Z axes are taken as the applied electric field direction and the layer normal, respectively.

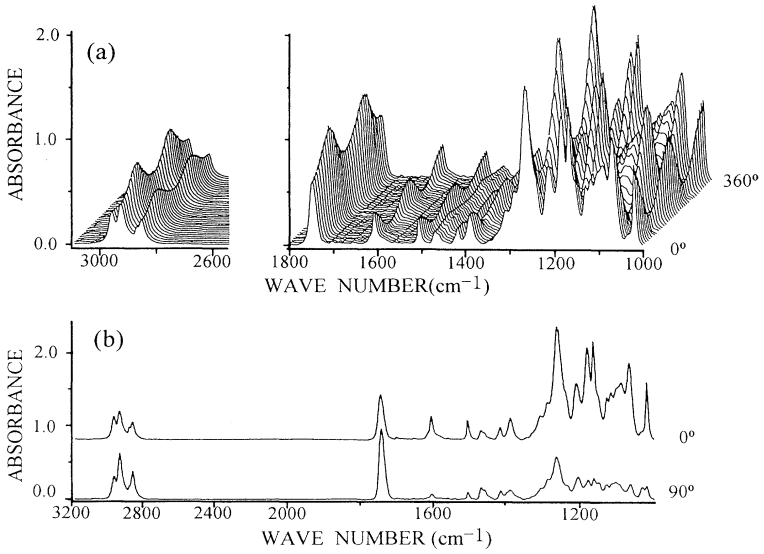

FIG. 2. Polarized ir spectra as a function of the rotation angle ω in Sm-A (70 °C) of homogeneously aligned TFMHPODB. Here ω is the angle between the polarization direction of an incident radiation and the smectic layer normal, and is taken as zero when these two directions coincide with each other.

TABLE II. The assignments of several peaks in infrared spectrum of TFMHPODB.

Observed frequencies /cm^{-1}	Assignments
2960	CH_3 degenerate asymmetric stretching
2929	CH_2 asymmetric stretching
2856	CH_2 symmetric stretching
1743	C=O stretching
1604,1504	phenyl ring C—C stretching
1465	CH_2 scissor vibration
1260	asymmetric C—O stretching
1180	aromatic CH in-plane deformation

CH_2 asymmetric stretching

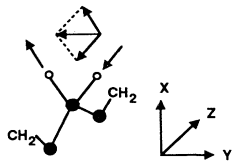

CH_2 symmetric stretching

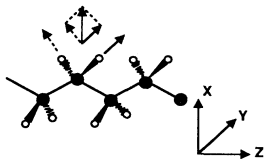

CH_2 scissor vibration

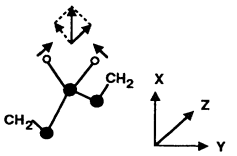

Phenyl ring stretching (1604 cm^{-1})

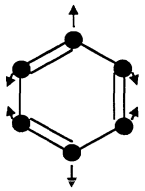

Phenyl ring stretching (1504 cm^{-1})

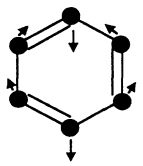

Aromatic CH in-plane deformation

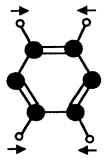

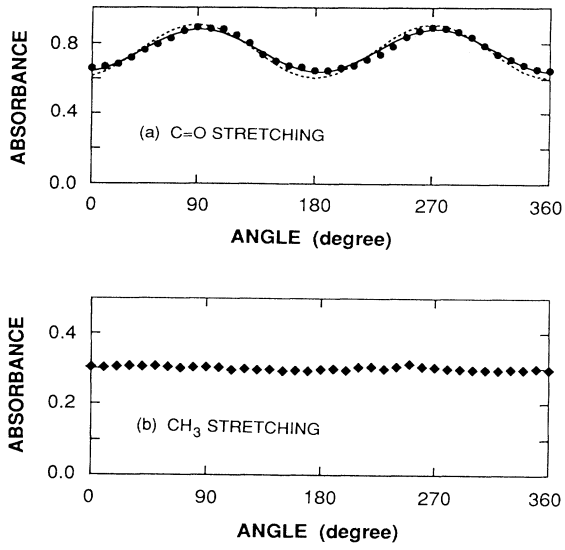

FIG. 3. Angular dependence of the absorbance for the C=O and CH_3 stretching peaks in Sm-A of homogeneously aligned TFMHPODB. For an explanation of solid and dotted curves, see Sec. IV B of the text.

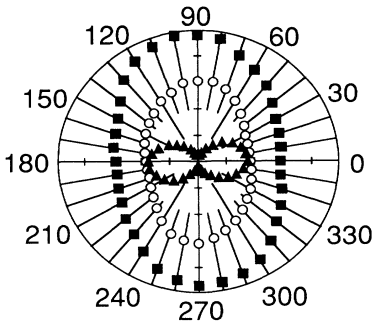

FIG. 4. Circular graphs of the absorbance vs the polarizer rotation angle ω for the phenyl ring (▲) and CH_2 (○) and C=O (■) stretching peaks in Sm-A of homogeneously aligned TFMHPODB.

rotation angle of ω. The dependence is classed under three types. The two phenyl ring stretching peaks at 1604 and 1504 cm^{-1} belong to the first type. The absorbances attain their maxima when the polarization direction of incident radiation coincides with the layer normal direction, $\omega=0°$ or 180°; the peaks show large dichroisms of $D=7.98$ and 5.10, respectively. This result indicates that the average stretching direction of phenyl rings is parallel to the long molecular axis, and that the stretching directions of the two phenyl rings nearly coincide with each other, as already mentioned in a previous paper [26].

In contrast to the phenyl peaks, the CH_2 peaks at 2929, 2856, and 1465 cm^{-1} belong to the second type. The absorbances attain their maxima at $\omega=90°$ or 270°. This fact is consistent with assignments shown in Table II in which the transition moments responsible for the CH_2 peaks are perpendicular to the alkyl chain C—C bond. The CH_2 peaks show relatively little absorbance variation with the polarizer rotation angle ω. The C=O stretching peak also belongs to the second type. Although the transition moments responsible for the C=O peak may not be perpendicular to the molecular long axis, the absorbance maximum appears at $\omega=90°$ or 270° because of the free rotation and the head-and-tail equivalence, as will be discussed below in detail. The absorbance variation with ω of the C=O peak is not large, either.

The third type of polarization dependence is observed in the CH_3 stretching peak, where the absorbance scarcely depends on ω. This isotropic character of the CH_3 peak may originate from the following three facts: (1) There are three CH_3 groups; (2) one of them rotates freely on the long molecular axis; and (3) the other two located at the end of the flexible carbon chains are fluctuating. In the following we will mainly focus our attention on the phenyl ring, CH_2 asymmetric, and C=O stretching peaks, since these are isolated from other peaks, unlike the low frequency peaks below 1300 cm^{-1}, and their assignments are unambiguous. Moreover, as will become clear in Sec. III B, these three are classed under the different types of polarization dependence in Sm-C^*, although two of them, the CH_2 and C=O stretching peaks, belong to the same type in Sm-A.

B. Polarized ir spectra in helicoidal Sm-C_A^* and unwound, uniform Sm-C^* observed using homogeneously aligned cells

Figures 5–8 summarize the absorbance as a function of ω for the three representative peaks, i.e., phenyl ring stretching (▲), CH_2 asymmetric stretching (○) and

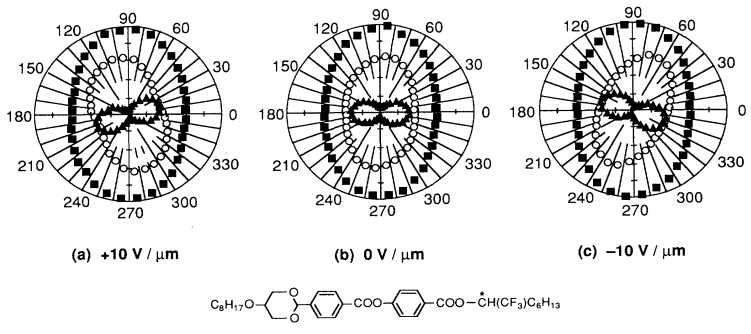

FIG. 5. Circular graphs of the absorbance vs the polarizer rotation angle ω for three representative peaks, phenyl ring (▲), CH_2 (○), and C=O (■) stretching, in Sm-C_A^* ($T=50$°C) of homogeneously aligned TFMHPODB under the application of dc electric fields; (a) +10 V/μm, (b) 0 V/μm, and (c) −10 V/μm.

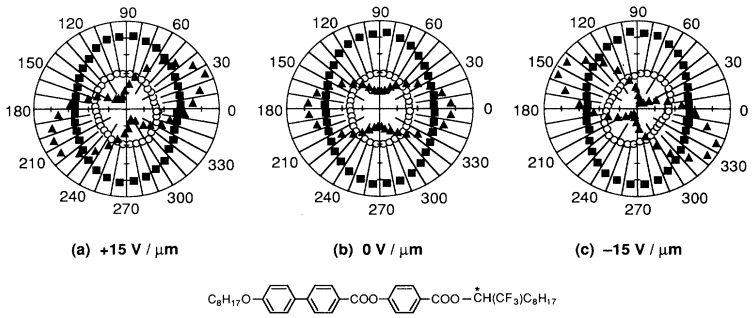

FIG. 6. Circular graphs of the absorbance vs the polarizer rotation angle ω for three representative peaks, phenyl ring (▲), CH_2 (○), and C=O (■) stretching, in Sm-C_A^* ($T=80$ °C) of homogeneously aligned TFMNPOBC under the application of dc electric fields: (a) +15 V/μm, (b) 0 V/μm, and (c) −15 V/μm.

C=O stretching (■ and □) peaks of the four compounds listed in Table I. In helicoidal Sm-C_A^* at zero electric field shown in (b) of Figs. 5–8, ω_{max}'s of the phenyl ring and CH_2 stretching, at which the maximum absorbances are obtained, appear in the same directions as in Sm-A. Due to the helicoidal structure in Sm-C_A^*, however, the maximum absorbances of the phenyl and CH_2 peaks decrease about 15 and 10%, respectively, and the minimum absorbances increase slightly. Note that ir absorbance is proportional to the square of the transition moment projection onto the polarization direction of the incident radiation.

By applying an electric field stronger than the threshold, ω_{max}'s of both the phenyl and CH_2 peaks rotate by the tilt angle $\pm\theta$ in Sm-C^*, i.e., about 25° at 50 °C in TFMHPODB, 30° at 80 °C in TFMNPOBC, 35° at 80 °C in TFMHPDOPB, and 22° at 105 °C in MHPOBC, as shown in (a) and (c) of Figs. 5–8. These ω_{max} changes imply the field induced phase transition from helicoidal Sm-C_A^* to unwound, uniform Sm-C^*. The reorientation of molecules to a direction parallel to the substrate surface brings about an absorbance increase at ω_{max} as well as an absorbance decrease at ω_{min} up to almost the same values in Sm-A. Note that ω_{max} of the CH_2 peak always occurs perpendicularly to ω_{max} of the phenyl peak. Although it is not given in Figs. 5–8, the CH_3 peak scarcely shows any ω dependence even in unwound Sm-C^*. In this way, the three types of polarization dependence in Sm-A are also observed in Sm-C^*.

A characteristic feature in Sm-C^* is that there exists a fourth type of polarization dependence. The one for the C=O peak shown in (a) and (c) of Figs. 5–8 is not symmetric with respect to ω_{max} of the phenyl peak. This is most clearly seen in MHPOBC (Fig. 8), where the two C=O's, the one in the chiral part and the other in the core part, give absorption peaks at 1720 and 1739 cm^{-1}, respectively. Upon the application of an electric field stronger than the threshold, ω_{max} of the 1720-cm^{-1} chiral C=O peak rotates by an angle much less than the tilt angle, and ω_{max} of the 1739-cm^{-1} core C=O peak hardly rotates. The absorbance at ω_{max} is smaller in the 1720-cm^{-1} chiral C=O peak than in the 1739-cm^{-1} core C=O peak. In the remaining three compounds which contain CF_3 instead of CH_3, the C=O stretching peaks due to the two carbonyls are not separated, and ω_{max} of the resulting C=O peak does not rotate when applying an electric field stronger than the threshold. The existence of this fourth type of polarization dependence is interesting because it suggests the hindered rotation of C=O groups on the long molecular axis, as will be discussed in Sec. IV B.

C. Polarized ir spectra in helicoidal Sm-C^* and unwound, uniform Sm-C^* observed using homeotropically aligned cells

Figures 9(a) and 9(b) show the angular variations of the four absorbance peaks measured in Sm-C^* of a homeotropically aligned MHPOBC cell using ir radiation incident perpendicularly to the substrate surface along the smectic layer normal; $\omega=0°$ is taken as the direction of an applied electric field. A helicoidal structure exists in Sm-C^* at zero electric field, and hence the absorbances of the phenyl peak at 1604 cm^{-1}, the CH_2 symmetric

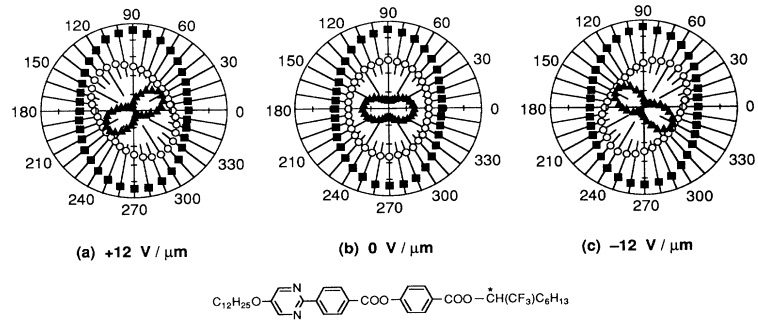

FIG. 7. Circular graphs of the absorbance vs the polarizer rotation angle ω for three representative peaks, phenyl ring (▲), CH_2 (○), and C=O (■) stretching in Sm-C_A^* ($T=80$ °C) of homogeneously aligned TFMHPDOPB under the application of dc electric fields: (a) +12 V/μm, (b) 0 V/μm, and (c) −12 V/μm.

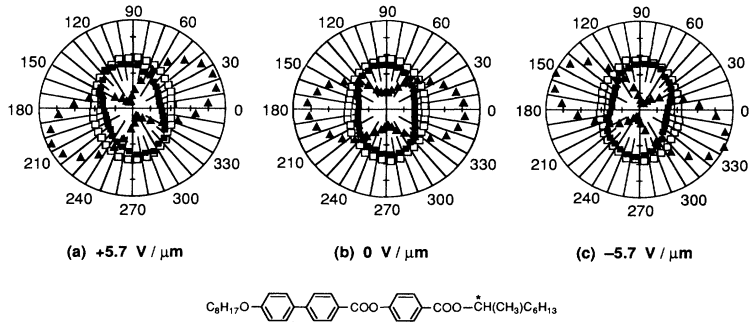

FIG. 8. Circular graphs of the absorbance vs the polarizer rotation angle ω for phenyl ring (▲), core C=O (□), and chiral C=O (■) stretching peaks in Sm-C_A^* ($T=105\,^\circ$C) of homogeneously aligned MHPOBC under the application of dc electric fields: (a) +5.7 V/μm, (b) 0 V/μm, and (c) −5.7 V/μm.

stretching peak at 2856 cm^{-1}, and the two C=O peaks at 1739 and 1720 cm^{-1} do not vary with ω. When applying a dc electric field of 75 V/mm, the angular dependence of the phenyl peak appears conspicuously; the intensity varies sinusoidally with its maximum at $\omega=90^\circ$ or 270°, i.e., in the polarization direction perpendicular to the electric field. Even in unwound, uniform Sm-C^*, the 1739-cm^{-1} core C=O peak scarcely changes its absorbance with ω. The 1720-cm^{-1} chiral C=O peak, on the other hand, shows a small angular dependence; the peak attains its maximum at $\omega=0^\circ$ or 180°, which is 90° out of phase with the 1604-cm^{-1} phenyl peak. The 2856-cm^{-1} CH_2 peak also shows an absorbance change with ω, though very small, and the peak attains its maximum at $\omega=0^\circ$ or 180°.

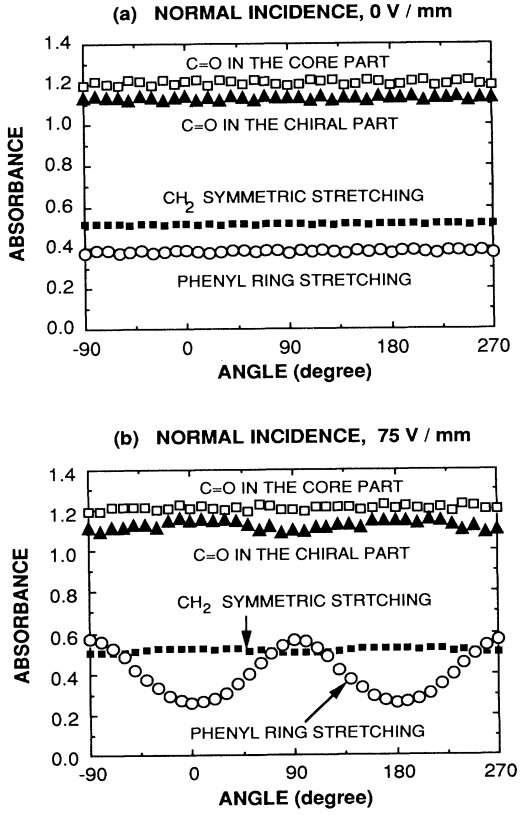

FIG. 9. Angular dependences of several absorbance peaks for normal incidence in Sm-C^* of homeotropically aligned MHPOBC at (a) $E=0$ V/mm and (b) $E=75$ V/mm. The electric-field direction is taken as $\omega=0^\circ$.

To confirm these small angular dependences of the chiral C=O and CH_2 peaks, the polarized ir spectra were measured using ir radiation obliquely incident along the long molecular axes, as shown in Fig. 1(c). Namely, a homeotropically aligned cell was rotated on an axis parallel to the applied electric field by a tilt angle of about 14° in Sm-C^*. The resultant spectra and its angular dependence of several peaks under the application of ±75-V/mm dc electric field are given in Fig. 10. In the positive electric field, the phenyl peak naturally shows a conspicuous angular dependence; the CH_2 peak also shows a small, 90° out of phase angular dependence. In the negative electric field, where the propagation direction of incident radiation is parallel to the average stretching direction of the phenyl ring, i.e., the long molecular axis, the phenyl peak apparently does not depend on ω, and its absorbance naturally decreases as compared with the value in the positive electric field. This independence of ω assures that the cell is mounted properly, so that the incident radiation actually propagates along the average long molecular axis. Even in this geometry, at least the 1720-cm^{-1} chiral C=O peak clearly shows an angular dependence. Note, however, that the angular dependence of the CH_2 peak at −75 V/mm naturally becomes less conspicuous than that at +75 V/mm.

D. Time-resolved ir spectra observed using homogeneously aligned cells

To explore the possibilities of observing conformational and orientational changes during tristable switching, i.e., the electric-field-induced phase transition between Sm-C_A^* and Sm-C^*, time-resolved spectra were obtained using a homogeneously aligned TFMHPODB. The peak absorbances are plotted as a function of delay time in Fig. 11; the optical response, i.e., the transmittance change, is also given together with the applied voltage. A pulsed electric field was applied for 40 μs and the spectra were measured from 0 to 85 μs at time intervals of 1.5 μs. The polarizer was set at 45° to the layer normal in order to obtain large intensity changes. The response time of TFMHPODB for the phase transition from Sm-C^* to Sm-C_A^* is 5–15 times faster than the other liquid crystals

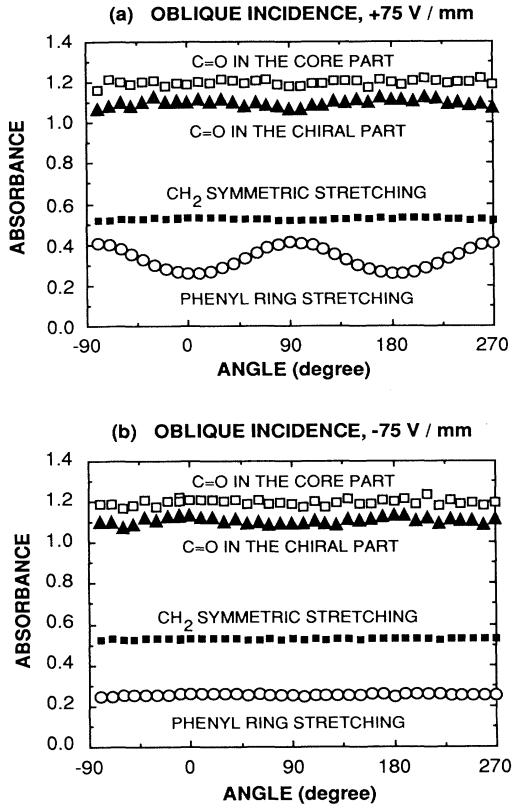

FIG. 10. Angular dependences of several absorbance peaks for oblique incidence in Sm-C^* of homeotropically aligned MHPOBC at (a) $E=+75$ V/mm and (b) $E=-75$ V/mm. The electric-field direction is taken as $\omega=0°$.

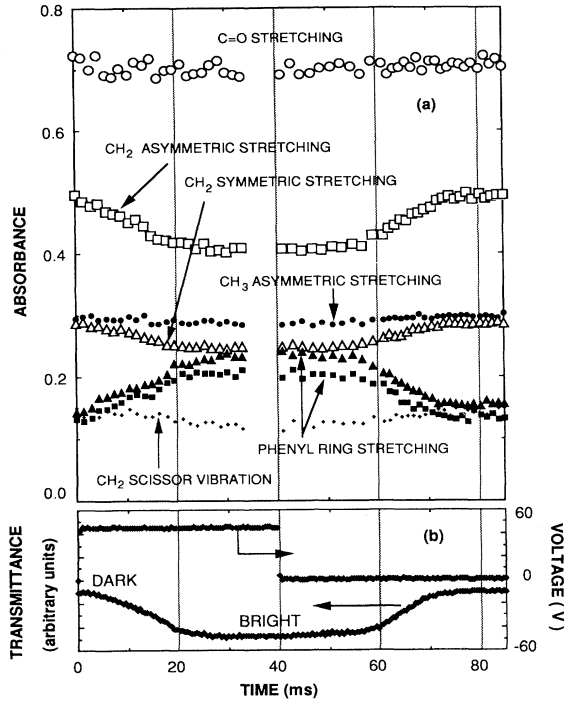

FIG. 11. Temporal absorbance variations of several peaks together with the optical response in Sm-C_A^* of homogeneously aligned TFMHPODB.

used in this experiment, so that the signal to noise ratio of spectra can be improved by increasing the frequency of an applied electric field up to 1 kHz.

The C=O and CH_3 stretching peaks do not show any absorbance changes during the switching, as already explained in Sec. III B. The absorbances of phenyl and CH_2 peaks start to change immediately after the electric-field application, and stop changing in nearly 25 μs. The relaxation process from Sm-C^* to Sm-C_A^*, on the other hand, does not occur immediately after turning off the electric field; it requires an induction period before the actual changes begin to occur. The induction period is approximately 15 μs, and the transition is completed in about 35 μs after the electric field was removed. These absorbance variations with time are completely consistent with the optical response [27]. From our time-resolved ir measurement with microsecond time resolution, we cannot find any differences in reorientation rates between alkyl and phenyl groups, contrary to several reports which contend that the alkyl chains respond much more quickly than the phenyl part in nematic liquid crystals [11,13,16] through the internal rotation on the C(biphenyl)—C(alkyl) bond. Therefore, it is considered that the phenyl and alkyl groups in antiferroelectric liquid crystals reorient simultaneously in the microsecond time scale at the phase transition between unwound Sm-C^* and Sm-C_A^*.

IV. DISCUSSION

A. Orientation of alkyl chains which is inconsistent with the zigzag model

One of the ordinary conclusions drawn from Figs. 3 and 4 is that the average stretching direction of phenyl rings is parallel to the molecular long axis, and that its orientational order is fairly high;

$$S=\langle \tfrac{1}{2}(3\cos^2\theta-1)\rangle=\frac{D-1}{D+2}\approx 0.7\ . \tag{1}$$

The lower orientational order of alkyl chains is another well-known conclusion. The smaller angular variations of the CH_2 peak result from the facts that there exist two alkyl chains which contain many CH_2 molecular segments and that the alkyl chains are thermally fluctuating. A conclusion drawn from Figs. 5–7 is that the orientational distribution of the transition moments responsible for the CH_2 peaks is cylindrically symmetrical with respect to the director (ω_{max} of the phenyl peak) even in unwound Sm-C^*, since ω_{max} of the CH_2 peak also rotates by the tilt angle $\pm\theta$, depending on the polarity of the applied electric field. This distribution is inconsistent with the so-called zigzag model, in which the two alkyl chains are considered to remain almost perpendicular to the lay-

ers, while the central rigid part of the molecules tilts in Sm-C^* [6,28,29].

B. Rotation of carbonyl groups, free in Sm-A and hindered in Sm-C^*

The transition moments responsible for the C=O stretching peak must make a definite polar angle β with respect to the phenyl ring stretching direction. X-ray analysis or molecular orbital calculation for several ester compounds suggests that $\beta \approx 60°$ [30,31]. Since the stretching direction of the phenyl rings is considered to be parallel to the long molecular axis on the average [26], we will assume in Sm-A that the C=O groups rotate freely on the molecular long axis, and that the axis fluctuates around the smectic layer normal with the order parameter S. Then the absorbance of the C=O stretching peak is given by [32]

$$A(\beta,\omega)=k\left\{\frac{S}{2}\sin^2\beta+\frac{S}{2}(2-3\sin^2\beta)\cos^2\omega+\frac{1-S}{3}\right\}, \tag{2}$$

where ω is the angle between the polarization direction of the incident radiation and the layer normal. In Fig. 3, the solid and dotted lines represent curves fitted by Eq. (2) with $\beta=60°$ and $S=0.7$ and with $\beta=60°$ and $S=1$, respectively; the proportional constant k was so chosen that the deviation is at a minimum. In this way, the free rotation model of the C=O groups appears to be quite reasonable in Sm-A.

In Sm-C^*, on the other hand, it is impossible to understand the C=O peak polarization dependence by assuming the free rotation of C=O groups. If they rotate freely on the long molecular axis, the angular dependence of the C=O peaks should be symmetrical with respect to the director (ω_{max} of the phenyl peak). Actually, however, this is not the case, not only in the chiral C=O group but also in the core C=O group, as is clear in Figs. 5–8. In addition, the asymmetry becomes more prominent as the tilt angle in Sm-C^* increases. Orientations in which the probability of finding the chiral C=O group reaches a maximum are illustrated schematically in Fig. 12. This illustration naturally explains that ω_{max} is almost parallel to the smectic layer. Fairly large absorbance at ω_{min} also suggests that the hindrance is not complete. Although the most probable orientation of each individual chiral C=O group is not in the plane containing the C_2 axis of Sm-C^* (the Y axis), the spontaneous polarization appears along the C_2 axis perpendicularly to the tilting plane because of the head-and-tail equivalence.

The C=O group rotation is biased not in a unique direction, but in the two directions illustrated in Fig. 12. This fact makes it difficult to confirm the hindrance by observing the polarization angular dependence using ir radiation propagating along the director, i.e., the average direction of the long molecular axis (see Fig. 10). Figure 13 shows the polarization angular dependence of the C=O peak, calculated by assuming that the rotation is biased completely and that the C=O group is located in two directions only. When the C=O group is located at

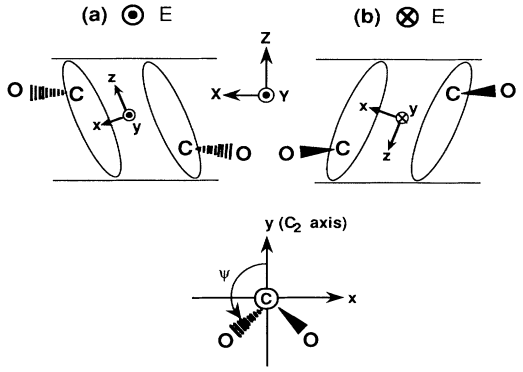

FIG. 12. Schematically illustrated orientation under electric fields of opposite polarity, in which the probability of finding the chiral C=O group becomes maximum. The z and y axes of the molecular frame are taken as the long molecular axis and the twofold C_2 axis, respectively, while the Z and Y axes of the laboratory frame are the layer normal and the C_2 axis, respectively. Reversing the electric-field polarity corresponds to the 180° rotation on the X axis.

$\psi=\pm 45°$ ($\pm 135°$), it is isotropic in spite of complete hindrance; here ψ is an angle between the y axis and the projection of C=O on the x-y plane. Conversely, the extremely small angular dependence does not simply mean the nearly free rotation of the C=O group. The asymmetrical angular dependence of the C=O group with respect to the director (see Figs. 5–8) clearly indicates that its rotation is biased.

As mentioned above, the polarization dependence of the C=O peak absorbance depends not only on the degree of hindrance but also on the spatial position of the C=O group (see Figs. 12 and 13). It is also true that the core C=O group rotation is hindered for the same reason that the angular dependence of the core C=O peak is not symmetric with respect to the director. The different angular dependence between the two C=O groups in MHPOBC, as shown in Fig. 8, may result from

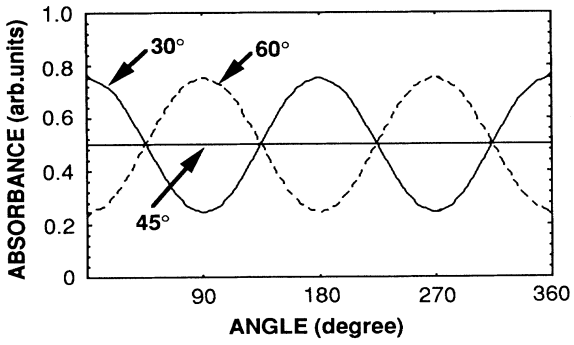

FIG. 13. Calculated polarization dependence of C=O peak assuming that the rotation about the long molecular axis is completely biased. The indicated angles 30°, 45°, and 60° are the rotation angle of C=O group about the long molecular axis ψ in Fig. 12.

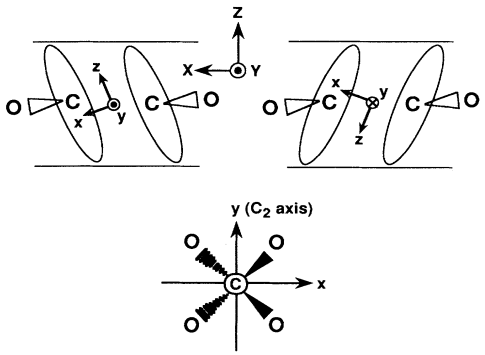

FIG. 14. Schematically illustrated orientation, in which the probability of finding the core C=O group reaches a maximum. The orientational distribution is assumed to be mirror symmetric with respect to the tilting plane. The molecular and laboratory frames are the same as in Fig. 12.

the difference in the most probable directions of the C=O groups. Moreover, the orientational distribution of the core C=O group may be mirror symmetric with respect to the tilting plane, as illustrated in Fig. 14, though hindered. Although absorbance dichroism measurements alone cannot decide the existence or nonexistence of this mirror symmetry, it is expected that the core C=O group, which is distantly separated from the chiral center, scarcely contributes to the spontaneous polarization.

In this way, the polarized FTIR spectroscopy gives microscopic proof, at least in its static aspect, of the hindered or biased rotational motion of carbonyl groups about the long molecular axis in the ferroelectric Sm-C^* phase. In connection with its dynamical aspect, experiments performed by Lalanne and co-workers [33–35] are interesting. They observed the relaxation time of the individual molecular rotational motion about the long axis by the degenerate four wave mixing technique; as the temperature approaches the Sm-A–Sm-C^* phase transition, the relaxation time becomes longer in Sm-A when the system is optically active, whereas it does not when the system is racemate. Note, however, that O'Brien *et al.* [36] could not find the critical behavior even in the optically pure material when they observed the optical Kerr effect. Lalanne, Buchert, and Kielich [35] criticized that, from the values of their optical Kerr effect amplitudes, O'Brien *et al.* did not probe the individual molecular rotational motion about the long axis as fast as ~10 ps. Instead, O'Brien *et al.* observed the collective one to be as slow as 100 ps–1 ns. This slow motion was also detected by dielectric spectroscopy [37]. The correlated molecular rotational motion thus observed did not show any critical slowing down, and hence does not appear to be related to the Sm-A–Sm-C^* phase transition. Note, however, that the slow relaxation time considerably slows down upon entering Sm-C [38,39]. To understand the rotational motion about the long molecular axis in more detail is one of the interesting future problems from the viewpoint toward elucidating the origin of ferroelectricity and antiferroelectricity in liquid crystals microscopically.

V. CONCLUSIONS

From polarized and time-resolved FTIR measurements, the following three conclusions were obtained.

(1) The stretching directions of phenyl rings nearly coincide with one another and are, on the average, almost parallel to the long molecular axis. The orientational distribution of the transition moments responsible for the CH_2 peaks is cylindrically symmetrical with respect to the long molecular axis; hence the molecular conformation in Sm-C^* is inconsistent with the so-called zigzag model.

(2) The C=O peak polarization dependence clearly indicates the hindered rotation of C=O groups about the long molecular axis. Although the most probable orientation of each individual chiral C=O group is not in the plane containing the C_2 axis of Sm-C^* (the Y axis), the spontaneous polarization appears along the two-fold axis of the C_2 point group to which Sm-C^* belongs, perpendicularly to the tilting plane because of the head-and-tail equivalence.

(3) For the field induced phase transitions between Sm-C^* and Sm-C_A^*, all the molecular segments reorient simultaneously on the microsecond time scale.

ACKNOWLEDGMENTS

We acknowledge the following companies for kindly supplying antiferroelectric liquid crystals used in the present study: Mitsubishi Gas Chemical Co., Inc., Showa Shell Sekiyu K. K., and Mitsubishi Chemical Corporation. This work was supported by a Grant-in-Aid for Scientific Research (Specially Promoted Research No. 06102005) from the Ministry of Education, Science and Culture.

[1] A. D. L. Chandani, T. Hagiwara, Y. Suzuki, Y. Ouchi, H. Takezoe, and A. Fukuda, Jpn. J. Appl. Phys. **27**, L729 (1988).

[2] A. D. L. Chandani, E. Gorecka, Y. Ouchi, H. Takezoe, and A. Fukuda, Jpn. J. Appl. Phys. **28**, L1265 (1989).

[3] A. Fukuda, Y. Takanishi, T. Isozaki, K. Ishikawa, and H. Takezoe, J. Mater. Chem. **4**, 997 (1994), and references therein.

[4] R. B. Meyer, L. Liebert, L. Strzelecki, and P. Keller, J. Phys. (Paris) **36**, L69 (1975).

[5] R. B. Meyer, Mol. Cryst. Liq. Cryst. **40**, 33 (1977).

[6] M. Koden, T. Kuratate, F. Funada, K. Awane, K. Sakaguchi, and Y. Shiomi, Mol. Cryst. Liq. Cryst. Lett. **7**, 79 (1990).

[7] T. Kusumoto, A. Nakayama, K. Sato, K. Nishide, T. Hiyama, S. Takehara, T. Shoji, M. Osawa, T. Kuriyama, K. Nakamura, and T. Fujisawa, J. Chem. Soc. Chem. Commun. **5**, 311 (1991).

[8] D. M. Walba, S. C. Slater, W. N. Thurmes, N. A. Clark, M. A. Handschy, and F. Supon, J. Am. Chem. Soc. **108**, 5210 (1986).

[9] P. Jacquinot, Rep. Prog. Phys. **23**, 267 (1960).

[10] K. Matsutani, H. Sugisawa, A. Yokota, Y. Furukawa, and M. Tasumi, Appl. Spectrosc. **46**, 560 (1992).
[11] T. Nakano, T. Yokoyama, and H. Toriumi, Appl. Spectrosc. **47**, 1354 (1993).
[12] A. Kaito, Y. K. Wang, and S. L. Hsu, Anal. Chim. Acta **189**, 27 (1986).
[13] H. Toriumi, H. Sugisawa, and H. Watanabe, Jpn. J. Appl. Phys. **27**, L935 (1988).
[14] H. Sugisawa, H. Toriumi, and H. Watanabe, Mol. Cryst. Liq. Cryst. **214**, 11 (1992).
[15] T. I. Urano and H. Hamaguchi, Chem. Phys. Lett. **196**, 287 (1992).
[16] T. I. Urano and H. Hamaguchi, Appl. Spectrosc. **47**, 2108 (1993).
[17] K. Matsutani, A. Yokota, Y. Furukawa, M. Tasumi, and A. Yoshizawa, Appl. Spectrosc. **47**, 1370 (1993).
[18] M. A. Czarnecki, N. Katayama, Y. Ozaki, M. Satch, K. Yoshino, T. Watanabe, and T. Yanagi, Appl. Spectrosc. **47**, 1382 (1993).
[19] A. Yasuda, K. Nito, and E. Matsui, Liq. Cryst. **14**, 1725 (1993).
[20] M. Johno, Y. Ouchi, H. Takezoe, A. Fukuda, K. Terashima, and K. Furukawa, Jpn. J. Appl. Phys. **29**, L111 (1990).
[21] N. B. Culthup, L. H. Daly, and S. E. Wiberley, *Introduction to Infrared and Raman Spectroscopy* (Academic, New York, 1975), Chaps. 8 and 9.
[22] W. O. George and P. S. Mcintyre, in *Infrared Spectroscopy,* edited by D. J. Mowthorpe (Wiley, New York, 1987), Chap. 7.
[23] G. Vergoten and G. Fleury, J. Mol. Struct. **30**, 347 (1976).
[24] A. Takase, S. Sakagami, and M. Nakamizo, Jpn. J. Appl. Phys. **17**, 1495 (1978).
[25] K. H. Kim, Y. Takanishi, K. Ishikawa, H. Takezoe, and A. Fukuda, Liq. Cryst. **16**, 185 (1994).
[26] K. H. Kim, K. Miyachi, K. Ishikawa, H. Takezoe, and A. Fukuda, Jpn. J. Appl. Phys. **33**, 5852 (1994).
[27] M. Johno, K. Itoh, J. Lee, Y. Ouchi, H. Takezoe, A. Fukuda, and T. Kitazume, Jpn. J. Appl. Phys. **29**, L107 (1990).
[28] R. Bartolino, J. Doucet, and G. Durand, Ann. Phys. **3**, 389 (1979).
[29] E. N. Keller, E. Nachaliel, D. Davidov, and C. Böffel, Phys. Rev. A **34**, 4363 (1986).
[30] J. P. Hummel and P. J. Flory, Macromolecules **13**, 479 (1980).
[31] P. Coulter and A. Windle, Macromolecules **22**, 1129 (1989).
[32] K. Toda, S. Nagaura and T. Watanabe, Nippon Kagaku Kaishi **3**, 459 (1975).
[33] J. R. Lalanne, J. Buchert, C. Destrade, H. T. Nguyen, and J. P. Marcerou, Phys. Rev. Lett. **62**, 3046 (1989).
[34] J. R. Lalanne, C. Destrade, H. T. Nguyen, and J. P. Marcerou, Phys. Rev. A **44**, 6632 (1991).
[35] J. R. Lalanne, J. Buchert, and S. Kielich, *Modern Nonlinear Optics,* edited by M. Evans and S. Kielich, Advances in Chemical Physics Series Vol. LXXXV (Wiley, New York, 1993), Pt. 1, p. 159.
[36] J. P. O'Brien, T. Moses, W. Chen, E. Freysz, Y. Ouchi, and Y. R. Shen, Phys. Rev. E **47**, 2269 (1993).
[37] B. Gestblom, M. Makrenek, W. Haase, and S. Wrobel, Liq. Cryst. **14**, 1069 (1993).
[38] J. A. Janik, J. Krawczyk, J. M. Janik, and K. Otnes, J. Phys. Colloq. **40**, 169 (1979).
[39] K. Chrusciel and W. Zajac, Liq. Cryst. **10**, 419 (1991).